



ISMEM 2017

- 2nd International Symposium on Multiscale
Experimental Mechanics: Multiscale Fatigue



A damage approach on the fatigue degradation mechanism of biaxial Glass/Epoxy laminates

Alexandros Antoniou, Christian Ueing, Catherine Lester, Nils Englisch

Materials Laboratory, Department of Materials and Structures, Division of Structural Components, Fraunhofer Institute for Wind Energy and Energy System Technology, Am Seedeich 45, 27572 Bremerhaven, Germany

e-mail: alexandros.antoniou@iwes.fraunhofer.de



Alexandros Antoniou is a mechanical engineer with a PhD in composite materials. He is holding the position of the technical director at the IWES accredited materials laboratory. He is working in developing and validating integrated material models in structural components with focus on wind turbine rotor blades.



Christian Ueing graduated in industrial engineering. He is working as a research associate at Fraunhofer IWES with a focus on mechanical characterisation of composite materials, test development and test validation.

Abstract

The fatigue stiffness reduction of a biaxial $[\pm 45]_{2s}$ glass/epoxy laminate was studied during tension-tension $R=0.1$ fatigue tests along the load direction and was correlated experimentally to the weighted crack density (ρ_w). Prismatic coupons were tested in displacement control at three separate strain levels, with a set limit for all test's end at 23% stiffness reduction. The ρ_w during fatigue was derived through an automated image analysis with an in-house software tool which implemented the Adaptive thresholding method with Gaussian weighting. A common stiffness degradation pattern was shown during the fatigue life for all the specimens when plotted in a normalized to unity scale. Moreover, a linear relation was revealed between ρ_w and the loss of fatigue stiffness, independent of the fatigue load level. An in-situ composite laminate fatigue remaining life prediction was augmented within a given uncertainty based on an experimental procedure through ρ_w measurements.

Introduction

The composite materials are well known to be damage tolerant. Well before their final catastrophic failure they experience extended micro which evolves to to macro scale damage. Early works in the quantification of damage accumulation addressed the term of crack density which is a crack number and sum value normalized on the corresponding area. In early 80's Kistner et al [1] published static test crack density measurements for cross-ply Carbon/Epoxy laminates, illustrating its evolution up to failure. Tong et al [2] studied cross-ply and quasi isotropic Glass/Epoxy laminates. It was noticed that the crack density behaviour was different between static and fatigue loading indicating for a strong influence on the load history. Adden et al [3] investigated the fatigue performance of non-crimp fabrics and proposed an analytical engineering approach for predicting the mechanical properties degradation. Multiaxial fatigue in multiaxial GI/Ep laminates was studied by the so called "Multiaxial Fatigue Team" [4], comparing the evolution of damage between uniaxially loaded prismatic coupons and tubular specimens under combined tension-torsion loadings. Implementing fracture mechanics simulations, they concluded that as long as the local biaxility stress ratios are the same, the damage evolution will be the same too. Carraro et al [6] proposed a procedure for the prediction of crack density evolution in multiaxial laminates under fatigue loads. The theoretical predictions were supported from experimental fatigue data results at R=0.05 ratio.

The multiaxial and specifically the biaxial ± 45 laminate configurations are very important for the wind turbine rotor blades. Although they are not the major load carrying laminates they cover large areas like the shear webs, the aerodynamic shells and flat-backs. Their operational integrity might not directly influence the blade stiffness and operation but potential stiffness degradation or strength limits might influence in the long run the panels stability and strength. The current work explores the damage initiation and propagation under fatigue loadings and correlates the crack density with the stiffness and the remaining life prediction.

Materials and manufacturing

All coupons were cut out of a cross-ply laminate consisting of a Saertex UD 1200 gr/m² fabric, with a relative angle of 45° to the UD0° and thus forming coupons with [+45/-45]_{2s} stacking sequence. The laminate fiber volume fraction was 53% on average. It was manufactured with the Vacuum Assisted Resin Transfer Moulding technique using Olin Airstone 880E resin, mixed with Olin Airstone 886H hardener in a 100:31 mass ratio. The plate was infused at 45°C, was cured for 20 hours at 45°C and was post-cured at 60°C for 10 hours. The heating rate was 1.25°/min. Peel plies were laid on both plate free surfaces.

Experiment

The coupons were tested under constant amplitude alternating loading (tension-tension $R=0.1$ displacement ratio) at a calibrated 25kN universal servo-hydraulic coupon machine under displacement control. The displacement measurement was performed through the machine integrated LVDT with an accuracy class of 0.5 according to DIN 51220. The environmental conditions were controlled i.e. temperature at $23^{\circ}\text{C}\pm 2^{\circ}$ and relative humidity at $50\%\pm 10\%$. A high resolution camera was installed at a fixed position on the coupon machine in front of the tested coupon, see Figure 1.

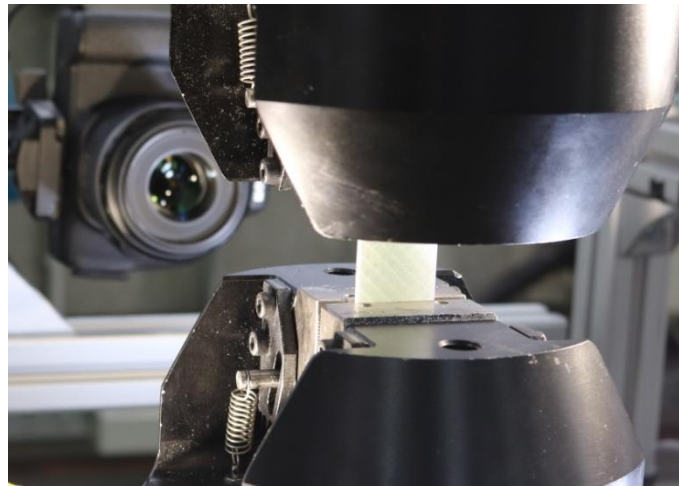


Figure 1. Experimental setup

The camera was shooting automated photos at 70% of the test maximum displacement, periodically at a specified amount of load cycles. The number was varying per test according to the expected total cycle number.

Load was also recorded during the tests, with an accuracy class of 0.5 according to DIN 51220. The coupon temperature was monitored at one side in the area next to the coupon machine grips. Therefore, a Pt100 thermocouple was used.

Nine prismatic coupons were tested at three separate strain levels, with a set end limit for all test's at 23% relative stiffness loss to each coupon's initial value.

The coupons were 127mm long and 25mm wide. They were clamped in the coupon machine without tabs and a free gauge length of 27mm. The list of the coupon nomenclature, the corresponding maximum coupon machine displacement as long as the test frequencies are summarized in the following Table.

Table 1. Summary of test parameters

Coupon ID	Frequency	Max. Displ.	*Max. Strain
(-)	(Hz)	(mm)	($\mu\text{m}/\text{m}$)
007	1	0,68	6800
008	1	0,68	6800
010-1	1	0,68	6800
005	2	0,54	5274
010	2	0,54	5274
011	2	0,54	5274
009	3	0,39	3661
011-1	3	0,39	3661
012-1	3	0,39	3661

* Max. strains were derived indirectly based on a comparison of the maximum displacement of the fatigue with a static test. In the static case the corresponding strain was measured with a strain gauge.

Analysis Tools

Stiffness degradation and Crack density

The fatigue stiffness (1) degradation of the biaxial glass/epoxy specimens was calculated along the tension-tension fatigue tests and was correlated to the weighted crack density (ρ_w) as defined in [5].

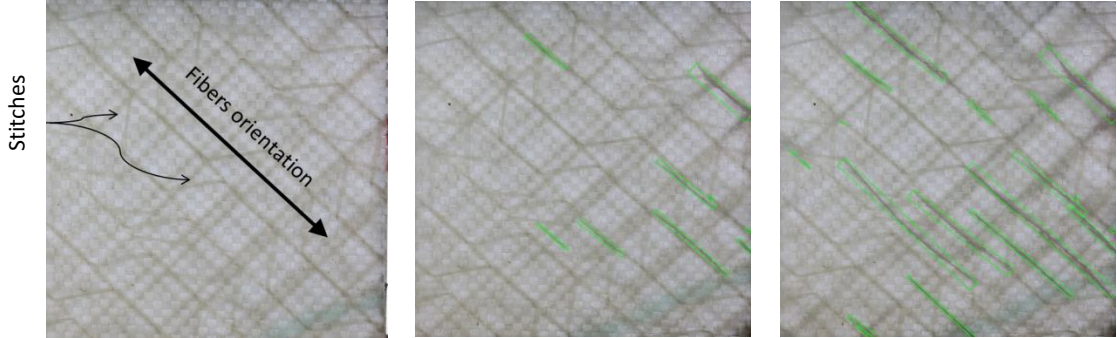
$$\text{Fatigue Stiffness} = \frac{\text{Force}_{\max} - \text{Force}_{\min}}{\text{Displ}_{\max} - \text{Displ}_{\min}} \quad (1)$$

$$\rho_w = \frac{\sum_{i=1}^n c_i}{wL} \quad (2)$$

c_i is the crack length, w is the observation width and L the observation length.

The weighted crack density was determined through an in-house software tool developed based on the openCV library [6]. An automated analysis was performed on images of the coupon gauge length surface (i.e. the laminate outermost ply), which were converted to black- white contrast implementing the Adaptive thresholding method with Gaussian weighting. The fabric pattern and stitching, shown in Table 2 were background, not cracks; therefore the initial image made during the first cycle was “subtracted” from subsequent images. This sequence highlighted the isolated cracks which were identified as contour shapes. When the shapes met certain criteria they were identified as green rectangular cracks. From these rectangle dimensions the length of each crack was subsequently calculated. Table 2 illustrates exemplarily sample images from three cycle levels and the crack accumulation derived from the in-house tool.

Table 2. Crack evolution over time and calculated weighted crack density through in-house software

Cycles	0	170.000	370.000
			
ρ_w	0	0,000778	0,002174

Results

Loss of Fatigue Stiffness (LFS)

The fatigue stiffness of the $[\pm 45]_{2s}$ laminate configuration was degrading during the fatigue tests. The absolute reduction during the fatigue tests for all the coupon data is summarized in Figure 2. The logarithmic cycle scale was selected in order to highlight the similarity of the degradation progress between the separate strain test levels. It also spotted two major zones (bi-linear performance), one where the stiffness loss was moderate and a second where the degradation is steeper.

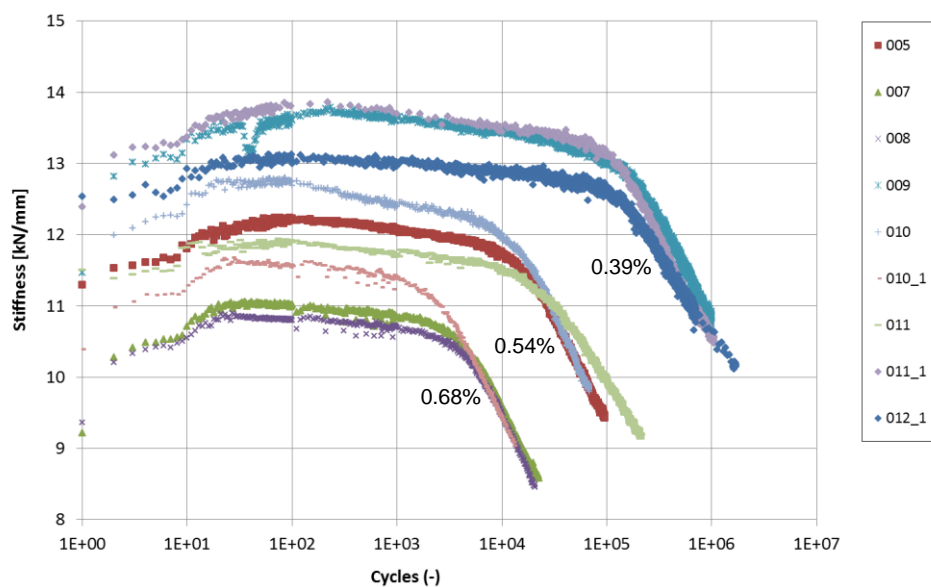


Figure 2. Summary of fatigue fatigue stiffness degradation (logarithmic cycle scale)

Plotting though the total Loss of Fatigue Stiffness vs. fatigue cycles in a normalised to unity graph, a common degradation performance is highlighted for all coupons. This means that by knowing the stiffness degradation at an arbitrary load it would be possible to predict the remaining fatigue life with a relative low uncertainty.

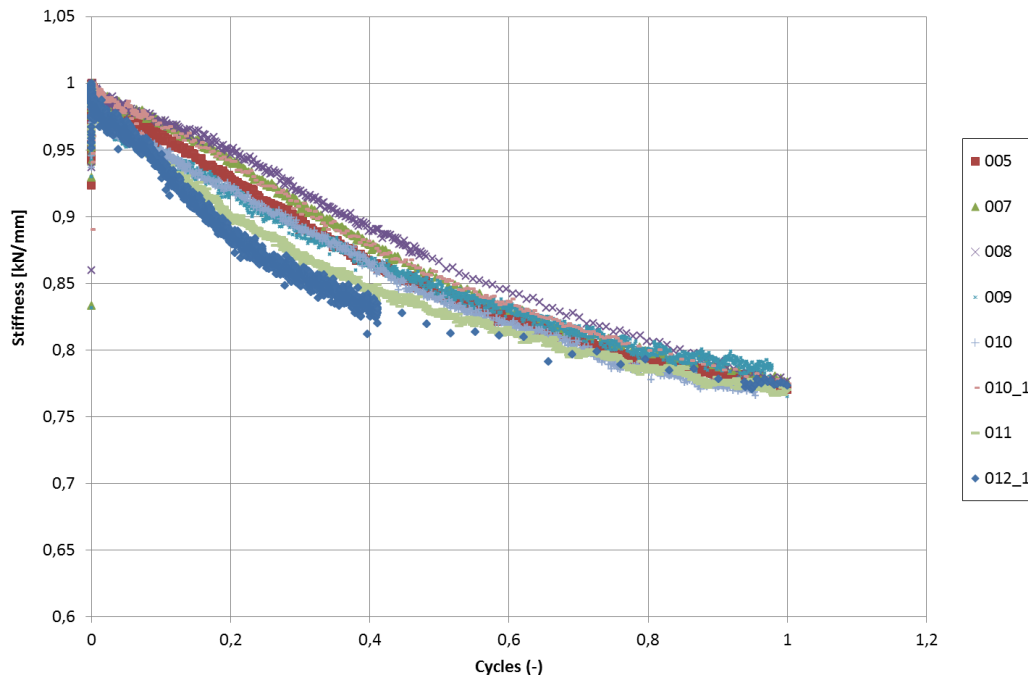


Figure 3. Summary of fatigue fatigue stiffness degradation (Normalized to unity, linear cycle scale)

The relative fatigue stiffness reduction in the load direction was correlated with the crack density recorded with the camera and analysed with the in-house software, as shown exemplarily in Figure 4 for coupon 005. The correlation was successful only when the first phase of the stiffness degradation was disregarded and the relative Loss of Fatigue Stiffness was calculated with reference the beginning of the second phase.

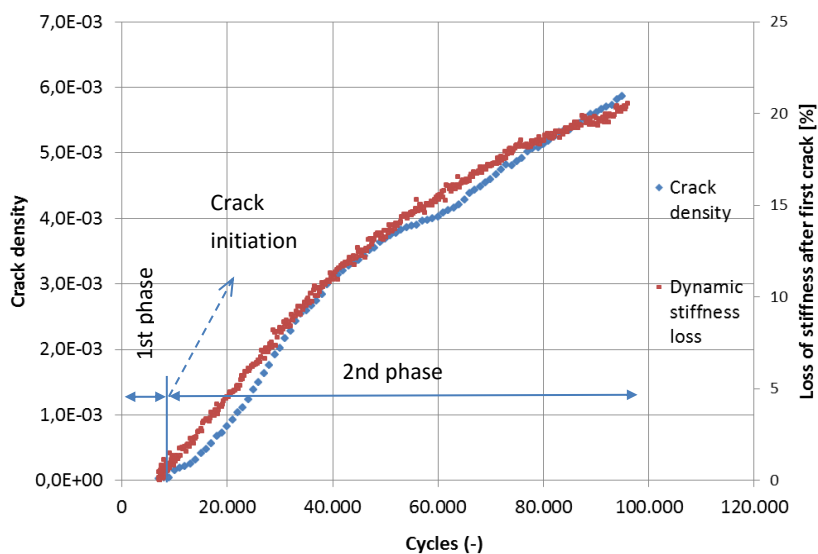


Figure 4. Crack density and Fatigue stiffness loss after first crack over fatigue cycles

Summarizing the results from all tests, see Table 3, it was shown that the first phase ended on an average of 3.27% reduction of the initial Fatigue Stiffness. The high coefficient of variation (COV) i.e. 37% was attributed to the limited amount of photos during the tests and therefore to the relative high uncertainty on the definition of the crack initiation cycle.

Table 3. Summary of test parameters

Coupon ID	Cycles to 1st crack	Cycles to 23% stif. Loss	*Stiffness Loss at 1 st crack	**Stiffness Loss after 1 st crack	*Stiffness Total Loss
(-)	(-)	(-)	(%)	(%)	(%)
007	1000	22600	3,28	20,55	22,99
008	1400	20400	1,91	20,95	22,40
010-1	400	13000	1,25	21,57	22,56
005	7000	96000	3,28	20,55	22,99
010	6000	68700	4,99	20,23	24,01
011	13000	214000	4,02	19,92	23,43
009	80000	1024057	5,12	19,82	24,28
011-1	70000	1055400	3,80	21,43	24,42
012-1	30000	1786200	2,81	21,12	25,97
Average			3,27	20,72	23,58
COV			0,37	0,03	0,04

* Calculated with reference to the experiment maximum stiffness ** Calculated with reference to the experiment stiffness at first crack

This means that although no cracks were identified, there was already small stiffness degradation of the laminate. Carraro et al. [7] was reporting of microcracks formation before the macrocrack propagation. Higher resolution cameras, Computer Tomography and smooth coupon surface could enhance the earlier identification. However, in the present research it was proved that the macrocracks were responsible for the initiation of the steep stiffness degradation phase.

In Figure 4 it was also shown that there is a linear relation between crack density and Fatigue Stiffness degradation after the first crack. This linear relation was proved in Figure 5 by plotting the two aforementioned parameters against each other. The results of the linear regression (3) on the experimental lines in order to determine parameters *a* and *b* are summarized in Table 4.

$$\text{Crack density} = a \cdot \text{LFS} + b \tag{3}$$

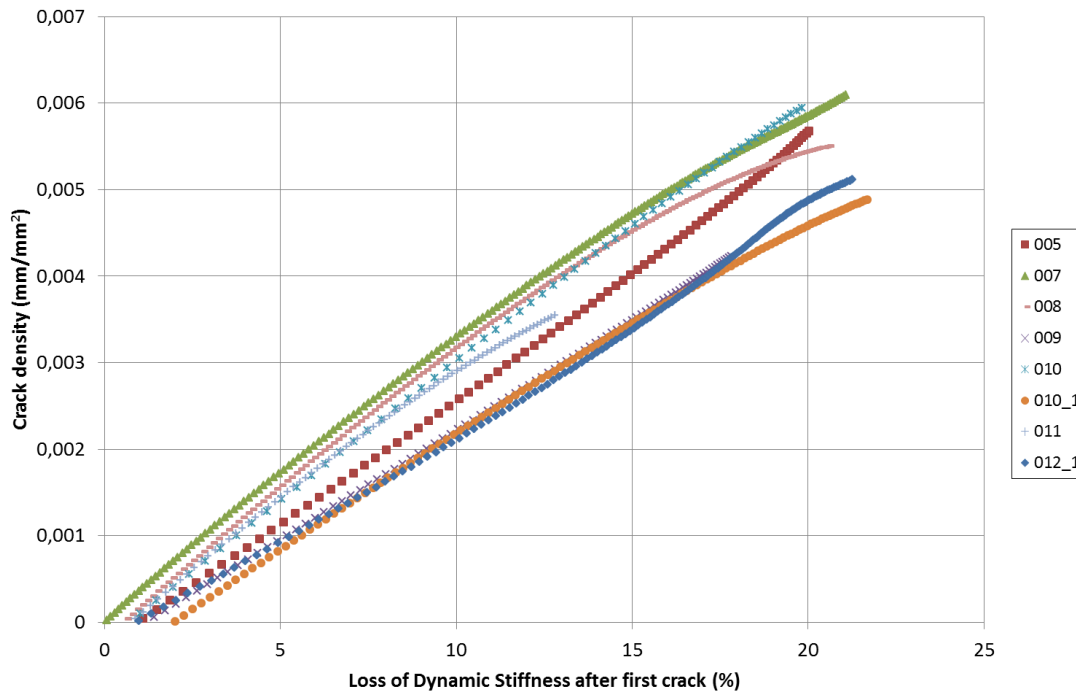


Figure 5. Summary of Crack density vs. Loss of Fatigue Stiffness after first crack

The 8% Coefficient of Variation of the slope a supports the assumptions that this remains constant for all the tests, irrespectively to the fatigue load level. The accuracy of parameter b is moderate. This had to do with mostly the accuracy of the method towards the 20% Loss of Fatigue Stiffness. The coupons then got relative dark due to the developed damage and it was not easy to distinguish the developed cracks with the software. Improving of the coupon surface i.e. manufacturing coupons with smooth surface is expected to reduce the experimental scatter.

Table 4. Summary of linear regression parameters of Crack Density vs. Loss of Fatigue Stiffness

Coupon ID	a	b
(-)	(-)	(-)
007	2,90E-04	3,00E-04
008	2,80E-04	1,60E-04
010-1	2,50E-04	-4,10E-04
005	3,00E-04	-3,60E-04
010	3,10E-04	-1,50E-04
011	3,00E-04	-9,00E-05
009	2,50E-04	-3,10E-04
011-1	Not valid	Not valid
012-1	3,00E-04	-4,00E-04
Average	2,85E-04	-1,58E-04
COV	0,08	-1,59

Case study

Assuming that only one linear regression curve represented the composite material fatigue performance and the correlation between crack density and loss of fatigue stiffness, and that there is no loss of stiffness without crack initiation, thus b parameter in formula (3) is neglected, the corresponding linear regression between crack density and LFS resulted into:

$$\text{Crack density} = 2,85 \cdot 10^{-4} \cdot \text{Loss of Fatigue Stiffness} \quad (4)$$

Moreover, it was supposed that there is a unique formulation which described the performance between normalized fatigue cycle (NFC) number and LFS. This was derived by averaging all the regression fit curves of all the experiments and is described below:

$$\text{Norm. Fat. cyc.} = 1,04 \cdot 10^{-4} \cdot \text{LFS}^3 - 1,73 \cdot 10^{-3} \cdot \text{LFS}^2 + 3,82 \cdot 10^{-2} \cdot \text{LFS} + 4,80 \cdot 10^{-2} \quad (5)$$

As a case study, based only on a given crack density of $3,82 \cdot 10^{-4}$ (exemplarily selected) which results in a Fatigue Stiffness loss of 13,4% according to (3), the corresponding normalized calculated fatigue cycles (5) for all coupons are summarized in Table 5. The NFC multiplied by the test cycles at 23% LFS resulted to the prognosis for the corresponding run cycles. The % differences of the calculated cycles from the experimental values derived through ρ_w are listed together with the prediction of the remaining life. It has to be noted that although the model is not conservative, the predictions are in a very good agreement with the test result.

Table 5. Fatigue cycle number at 13,4% Loss of Fatigue Stiffness: Calculation and tests

Coupon ID	Cycles to 23% LFS	NCF	Calculated cycles	Test cycles	Difference	Remaining life (calc.)	Remaining life (test)
(-)	(-)	(%)	(-)	(-)	(%)	(%)	(%)
007	22600	49,6	11199	10000	-12,0	50,4	55,8
008	20400	49,6	10109	10800	6,4	50,4	47,1
010-1	13000	49,6	6442	8100	20,5	50,4	37,7
005	96000	49,6	47572	53000	10,2	50,4	44,8
010	68700	49,6	34044	37500	9,2	50,4	45,4
011	214000	49,6	106047	110000	3,6	50,4	48,6
009	1024057	49,6	507466	860000	41,0	50,4	16,0
011-1	1055400	49,6	522998	740000	29,3	50,4	29,9
012-1	1786200	49,6	885141	845000	-4,8	50,4	52,7

Conclusions-Discussion

The damage evolution during tension-tension ($R=0.1$) displacement controlled tests of a $[\pm 45]_{2s}$ laminate was investigated. High resolution photos recorded the crack initiation and propagation transverse to the fiber direction. The images were processed through an

automated in-house tool and the amount of cracks was inverted to a crack density value. It was shown that the transverse cracks are responsible for the major part of the stiffness reduction of the laminate in the load direction. The evidence was that the evolution of the crack density was linearly related with the reduction of the Fatigue Stiffness. The overall stiffness reduction, before any crack was optically captured, was relative constant for all coupons, around 3%. This was attributed to possible microcracking effects. Additionally, the Fatigue Stiffness degradation was similar for all specimens when plotted over fatigue cycles in a normalized to unity scale. This fact augmented a direct correlation between the experimentally measured crack density and the prediction of the run cycle number ratio. In the case study that was presented, the correlation of the calculated cycles for a given value of crack density was in a very good correlation to the experimental results. Still though, the experimental scatter will have to be further investigated. The presented experimental methodology highlights the initiation of macrocracks and therefore gives input for validating failure criteria for Biax laminates. In case of fail safe and progressive damage design, it also provides with vital information on the stiffness degradation to be expected due to fatigue after the macrocrack initiation. It can be useful for a designer of composite structures providing with a residual fatigue life model.

Acknowledgements

The authors acknowledge the German Federal Ministry of Education and Research (BMBF) for funding the project LENA (project number: 03SF0529C).

References

1. Kistner MD, Whitney JM, Browning CE; First Ply Failure of Graphite/Epoxy Laminates; Proc. U.S.-Japan 1983
2. Tong J, Guild FJ, Ogin SL, Smith PA; On matrix crack growth in quasi-isotropic laminates-I. Experimental Investigation; Comp Sci Technol 57 (1997) 1527-1535
3. Adden S, Horst P; Stiffness degradation under fatigue in multiaxially loaded non-crimped-fabrics; Int J Fatigue 32 (2010) 108-122
4. Quaresimin M, Carraro PA, Mikkelsen LP, Lucato N, Vivian L, Brøndsted P, Sørensen BF, Varna J, Talreja R; Damage evolution under cyclic multiaxial stress state: A comparative analysis between glass/epoxy laminates and tubes; Compos Part B: 61 (2014) 282-290
5. Carraro PA, Maragoni L, Quaresimin M; Prediction of the crack density evolution in multidirectional laminates under fatigue loading; Comp Sci Technol 128 (2016) 147-154
6. Website: <http://opencv.org/>; Version: 2.4; Download date: 29.03.2017
7. Carraro PA, Maragoni L, Quaresimin M; A damage based model for crack initiation in unidirectional composites under multiaxial cyclic loading; Comp Sci Technol 99 (2014) 154-163